This article has been accepted for inclusion in a future issue of this journal. Content is final as presented, with the exception of pagination.

Remote Sensing Image Registration With Modified SIFT and Enhanced Feature Matching

Wenping Ma, Zelian Wen, Yue Wu, Licheng Jiao, *Senior Member, IEEE*, Maoguo Gong, *Senior Member, IEEE*, Yafei Zheng, and Liang Liu

***Abstract*—The scale-invariant feature transform algorithm and its many variants are widely used in feature-based remote sensing image registration. However, it may be difficult to find enough correct correspondences for remote image pairs in some cases that exhibit a significant difference in intensity mapping. In this letter, a new gradient definition is introduced to overcome the difference of image intensity between the remote image pairs. Then, an enhanced feature matching method by combining the position, scale, and orientation of each keypoint is introduced to increase the number of correct correspondences. The proposed algorithm is tested on multispectral and multisensor remote sensing images. The experimental results show that the proposed method improves the matching performance compared with several state-of-the-art methods in terms of the number of correct correspondences and aligning accuracy.**

***Index Terms*—Feature matching, image registration, remote sensing, scale-invariant feature transform (SIFT).**

I. Introduction

IMAGE registration is the process of matching two or more images of the same scene with different time, different sensors, and different viewpoints [1]. It is an indispensable part for many remote sensing tasks, such as change detection, image fusion, and environmental monitoring.

A number of methods have been proposed for remote sensing image registration. These methods can be coarsely partitioned into two categories: intensity-based methods and feature-based methods [1], [2]. Intensity-based methods use similarity between pixel intensities to determine the alignment between two images. Mainly used similarity measures are cross correlation and mutual information [2]. However, intensity-based methods suffer from monotonous textures [3], illumination differences, and a high degree of computational complexity of global optimization [4]. Feature-based methods extract salient features and use the correlation between those features to determine the optimal alignment. In general, these features include point, edge, contour, the centroid of a specific region [5], [6], and so on. Among the feature-based methods, the scale-invariant feature transform (SIFT) [7] is the classic algorithm. SIFT is invariant to image scaling and rotation and partially invariant to change in illumination and camera viewpoint, and it has been used successfully in registration of visible images. Some other improvements have been made in feature-based methods, such as SURF [8], GLOH [9], and BRISK [10]. These improvements are mainly to improve the computational efficiency. However, when SIFT is directly applied to remote sensing images, the number of correct correspondences is not enough to confirm matching accuracy [4] due to the significant difference in intensity mapping. The intensity mapping may be linear, nonlinear, and erratic. To overcome the problem, Li *et al.* [4] has proposed robust SIFT (R-SIFT), in which the gradient orientation of each pixel is refined, and more main orientations are assigned to each keypoint. In the process of feature matching, the scale–orientation joint restriction criterion is introduced to improve the matching performance. Kupfer *et al.* [11] proposed a fast mode-seeking SIFT (MS-SIFT) algorithm that exploits the scale, orientation, and position information of SIFT features, followed by the effective removal of imprecise SIFT keypoint correspondences. Sedaghat *et al.* [3] proposed the uniform R-SIFT (UR-SIFT) algorithm. The UR-SIFT method effectively generates enough robust, reliable, and uniformly distributed aligned keypoints. Gong *et al.* [2] proposed a coarse-to-fine scheme for automatic image registration. The coarse results provide a near-optimal initial solution for the optimizer in the fine-tuning process.

In this letter, we propose a new gradient definition to overcome the difference of image intensity between the remote image pairs. In addition, a robust point matching algorithm that combines the position, scale, and orientation of each keypoint to increase the number of correct correspondences is proposed. This algorithm is inspired by the SIFT algorithm and will be called PSO-SIFT. We assume a similarity transformation model, which is widely used in the registration of remote sensing images. In Section II, the outline of the classical SIFT algorithm and its limitations on remotely sensed images are discussed. The proposed algorithm in this letter is presented in Section III. The experiment results on three different remote sensing image pairs are illustrated in Section IV. Concluding remarks are provided in Section V.

II. Background

The SIFT-based registration algorithm consists of three main modules: keypoint detection, descriptor extraction, and keypoint matching. A difference of Gaussian scale space, as an approximation of the Laplacian of Gaussian, is constructed. Local extrema in the three dimensions are then selected as candidate keypoints. Each keypoint is assigned one or more main orientations based on a local histogram of gradient orientation. Then, a 128-element descriptor is assigned to each keypoint. The obtained SIFT feature comprises four components: local

Manuscript received January 7, 2016; revised June 12, 2016 and July 27, 2016; accepted August 9, 2016.

The authors are with the Key Laboratory of Intelligent Perception and Image Understanding of Ministry of Education, International Research Center for Intelligent Perception and Computation, Xidian University, Xi'an 710071, China (e-mail: wpma@mail.xidian.edu.cn; zelianwen@foxmail.com).

Color versions of one or more of the figures in this paper are available online at http://ieeexplore.ieee.org.

Digital Object Identifier 10.1109/LGRS.2016.2600858

1545-598X © 2016 IEEE. Personal use is permitted, but republication/redistribution requires IEEE permission.
See http://www.ieee.org/publications_standards/publications/rights/index.html for more information.

This article has been accepted for inclusion in a future issue of this journal. Content is final as presented, with the exception of pagination.

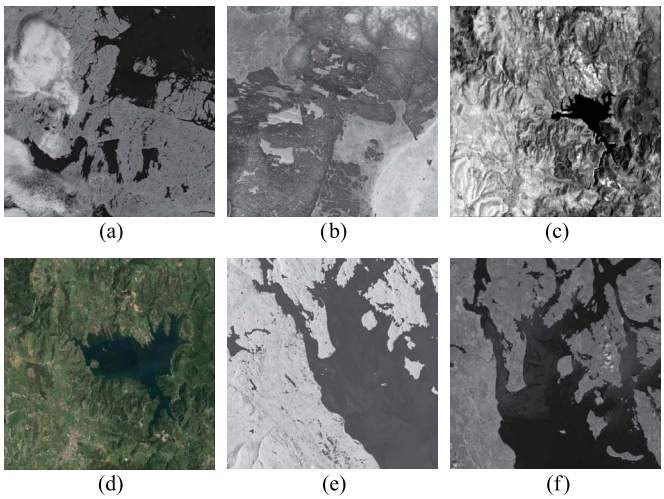

Fig. 1. Remote sensing image pairs. (a) Landsat-7 ETM+, band 5. (b) Landsat 4-5 TM, band 3. (c) Landsat TM, band 5. (d) Google earth, optical. (e) ALOS-PALSAR. (f) Landsat ETM+, band 5.

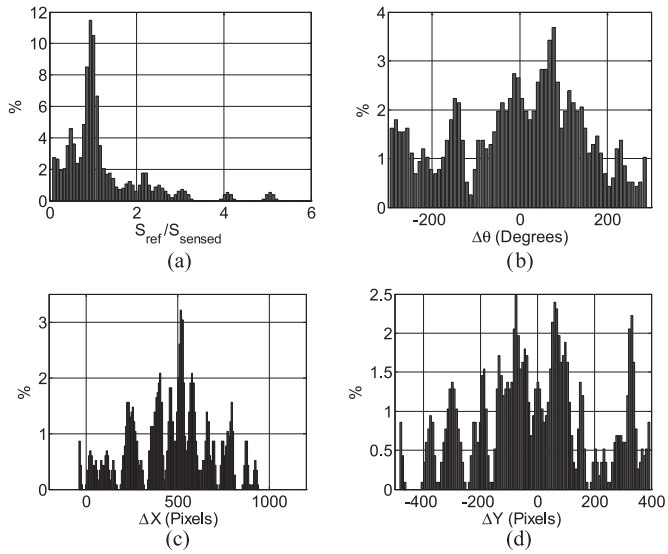

Fig. 2. (a)–(d) Histograms of scale ratio, main orientation difference, horizontal shifts, and vertical shifts.

(x_i, y_i), scale s_i, orientation θ_i, and descriptor d_i. The last module uses the minimum Euclidean distance on descriptors as the keypoint matching criterion. More details about SIFT can be found in [7].

Fig. 1(a) and (b) shows multispectral images that are acquired in two different bands and different sensor devices. Therefore, they have very different intensity mappings and are typically more difficult to register. Fig. 2 shows the histograms of the scale ratio, main orientation difference, horizontal shifts, and vertical shifts of the matched original SIFT keypoints in Fig. 1(a) and (b). The keypoints are matched by the ratio between the Euclidean distance of the nearest neighbor and that of the second nearest neighbor of corresponding descriptors. The threshold on the ratio is set to d_{ratio}. Detailed parameter setting of histograms can be found in [11]. We can see that the four histograms cannot evidently exhibit a single mode except for the scale ratio histograms, which, due to the difference of intensity mapping between the multispectral images and the same areas in multispectral remote images, could have a significant nonlinear intensity difference [4]. Such intensity difference will result in different main orientation difference of correspondences that are expected to be correctly matched. Moreover, the feature descriptors are not robust to these differences, because the main orientation of each keypoint is used in the process of descriptor extraction to ensure rotation invariance.

III. Proposed Method

A. New Gradient Definition

The significant difference of intensity mapping will result in different gradient orientations and gradient magnitudes of the same area between the remote sensing image pairs. Therefore, the SIFT correspondences that are expected to be correctly matched will not have a minimum Euclidean distance as the correspondence computation depends on the descriptor that is formed by gradient orientations and gradient magnitudes around the keypoint location. To make the descriptor more robust to such differences, we propose a new gradient definition (including orientation and magnitude) for each pixel in Gaussian scale space. To improve the efficiency of the proposed method, the input image pair is not expanded, and we use the original input image to building the lowest level of the Gaussian pyramid. First, we compute the gradient magnitude of the Gaussian scale-space image by means of Sobel filters as

$$G_\sigma^1 = \sqrt{\left(G_{x,\sigma}^1\right)^2 + \left(G_{y,\sigma}^1\right)^2} \tag{1}$$

where σ is the scale of Gaussian scale space, and $G_{x,\sigma}^1$ and $G_{y,\sigma}^1$ denote the horizontal and vertical derivatives of the Gaussian scale-space image with scale σ, respectively. Then, we define the proposed gradient orientation and gradient magnitude as

$$R_\sigma^2 = \arctan\left(\frac{G_{y,\sigma}^2}{G_{x,\sigma}^2}\right), \quad G_\sigma^2 = \sqrt{\left(G_{x,\sigma}^2\right)^2 + \left(G_{y,\sigma}^2\right)^2} \tag{2}$$

where $G_{x,\sigma}^2$ and $G_{y,\sigma}^2$ denote the horizontal and vertical derivatives of gradient magnitude image G_σ^1 of Gaussian scale space, respectively. All the derivatives are approximated by means of Sobel filters. Using the Sobel operator, the derivative [12], [13] is easily computed. Note that the gradients computed by (2) are used in the process of orientation assignment and descriptor extraction. In this letter, we do not use a Gaussian weighting of the gradient magnitudes when computing histograms [14]. Instead of using a square neighborhood and 4×4 square sectors as in the original SIFT descriptor, we use a GLOH-like [9], [14] circular neighborhood (radius of 12σ) and log-polar sectors (17 location bins) to create a feature descriptor. A series of experiments shows that GLOH obtains the best results [9]. Note that the gradient orientations are quantized in eight bins. This results in a 136-dimensional descriptor. Fig. 4(a) illustrates the approach.

Fig. 3 shows the histograms of the scale ratio, main orientation difference, horizontal shifts, and vertical shifts of the matched keypoints in Fig. 1(a) and (b) after applying the proposed gradient definition. In contrast to the results in Fig. 2, these histograms evidently exhibit a single mode except for the main orientation difference histogram that has two main modes. The reason why the main orientation difference histogram has two main modes is that the circumferential angle is not

This article has been accepted for inclusion in a future issue of this journal. Content is final as presented, with the exception of pagination.

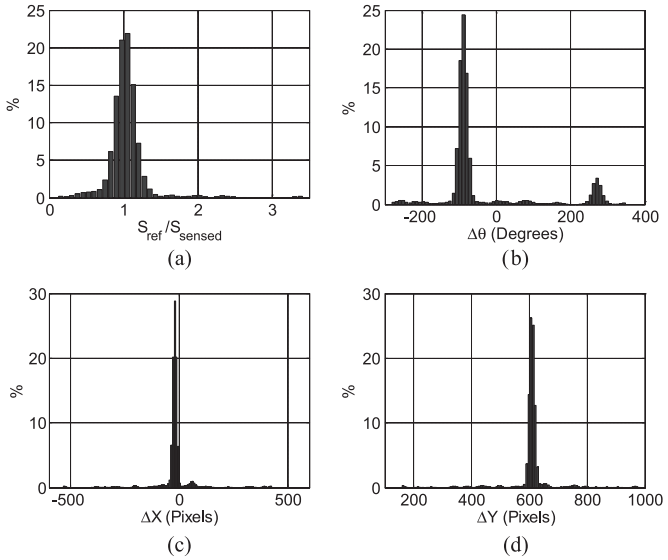

Fig. 3. (a)–(d) Histograms of scale ratio, main orientation difference, horizontal shifts, and vertical shifts.

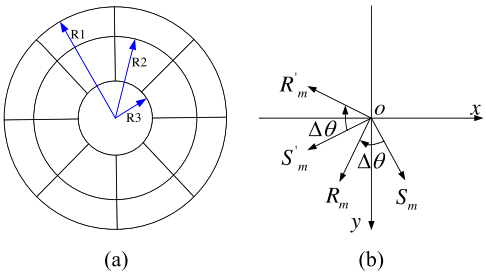

Fig. 4. Scheme of log-polar sectors and the mode of the main orientation difference. (a) Log-polar sectors. Parameter R1 is set to 12σ. Ratio of R3 and R2 to R1 is 0.25 and 0.73, respectively. (b) Two modes of the main orientation difference in numerical. Single mode of rotation angle in space.

continuous in -180° and 180° [see Fig. 4(b)]. It is necessary to point out that there is only one main mode in rotation angle. If we know one of the locations of the two main models, the location of another mode can be computed as

$$\Delta\theta' = \begin{cases} \Delta\theta + 360, & \Delta\theta \in [-360, 0) \\ \Delta\theta - 360, & \Delta\theta \in [0, 360) \end{cases} \tag{3}$$

where $\Delta\theta$ and $\Delta\theta'$ denote the locations of two modes of the main orientation difference histogram, respectively. Fig. 4(b) illustrates the two modes of the main orientation difference and the single mode of rotation angle. The mode of the scale ratio is easily located at $r = 1.022$. Two modes of the main orientation difference are located at $\Delta\theta = -89.61$ and $\Delta\theta' = 270.97$. The modes of horizontal shifts and vertical shifts are obtained at $\Delta x = -10.96$ and $\Delta y = 608.76$. Note that the exact location of the mode is obtained by an appropriate interpolation method [11]. The relationship between $\Delta\theta$ and $\Delta\theta'$ is very close to the results of (3). Finally, we employ the fast sample consensus (FSC) algorithm [15] to obtain the transformation model parameters $r = 0.99$, $\Delta\theta = -90$, $\Delta x = -9.71$, and $\Delta y = 604.75$, respectively. From the above results and analysis, it can be seen that the new gradient calculation method is better in dealing with the problem of intensity differences of remote sensing image pairs.

B. Enhanced Feature Matching

Similarity transformation consists of three parameters: translation, scale, and rotation. Under the similarity transformation model, the correct-match pairs will have the same rotation angle in space, the same scale ratio, the same horizontal shifts, and the same vertical shifts in most cases. Hence, we use the inherent information (i.e., position, scale, and main orientation) of each keypoint to increase the number of correct correspondences.

Two point feature sets $P = p_1, p_2, \ldots, p_M$ and $P' = p'_1, p'_2, \ldots, p'_N$ have been extracted from the reference and sensed images, respectively. (x_i, y_i), s_i, and θ_i denote the position, scale, and main orientation of the keypoint p_i, respectively, in the reference image. (x'_i, y'_i), s'_i, and θ'_i denote the position, scale, and main orientation of the keypoint p'_i, respectively, in the sensed image. The position transformation error of correspondence p_i and p'_i is denoted as

$$e_p(i) = \|(x_i, y_i) - T\left((x'_i, y'_i), \mu\right)\|$$

where $T((x'_i, y'_i), \mu)$ is the similarity transformation model, and μ is the transformation model parameter. We also use the scale error [4] and the relative main orientation error [4] of point p_i and p'_i as

$$e_s(i) = \left|1 - (r^*)\frac{s'_i}{s_i}\right|, \quad e_o(i) = \text{abs}(\Delta\theta_i - \Delta\theta^*)$$

where r^* and $\Delta\theta^*$ denote the mode locations of scale ratio and main orientation difference between reference and sensed images, respectively, and $\Delta\theta_i = \theta_i - \theta'_i$ denotes the main orientation difference between p_i and p'_i. Then, we define a more robust joint distance named position scale orientation Euclidean distance (PSOED) as

$$\text{PSOED}(i) = (1 + e_p(i))\,(1 + e_s(i))\,(1 + e_o(i))\,\text{ED}(i) \tag{4}$$

where $\text{ED}(i)$ denotes the Euclidean distance of the descriptors corresponding to the keypoints p_i and p'_i. The PSOED will be minimized in most cases when the point pairs are correctly matched. The proposed matching algorithm is given below.

1) *Initial matching:* The keypoints are matched by the ratio between the Euclidean distance of the nearest neighbor and that of the second nearest neighbor of corresponding descriptors. The threshold on the ratio is set to d_{ratio}. Pair set PP is obtained, and we set up the histograms of scale ratio, main orientation difference, horizontal shifts, and vertical shifts. The mode locations r^*, $\Delta\theta^*$, Δx^*, and Δy^* are obtained from the histograms. The FSC algorithm [15] is used to calculate the initial transformation parameter μ from pair set PP.
2) *Rematching:* As the main orientation difference histogram has two modes, there are only two different combinations of r^*, $\Delta\theta^*$, Δx^*, and Δy^*. For each mode combination, we use PSOED as the distance measure, and the keypoints are matched by the ratio between the distance of the nearest neighbor and that of the second nearest neighbor. The threshold on the ratio is denoted as d_r. Because matching is performed twice, the keypoints in the reference image or the sensed image will have one or more matching in another image; hence, we regard the point pair with the minimum PSOED as the

This article has been accepted for inclusion in a future issue of this journal. Content is final as presented, with the exception of pagination.

candidate matching pair. Then, a keypoint pair set PP_1 is obtained.

3) *Outlier removal:* There will be some false correspondences in PP_1. Hence, we first use the method proposed in MS-SIFT [11] to filter out most of the outliers. Let (x_1, y_1) and (x_1', y_1') denote the coordinates of corresponding keypoints in set PP_1. The horizontal and vertical shifts of corresponding keypoints are defined as

$$\begin{aligned}\Delta x_1 &= x_1 - r^* \left(x_1' * \cos(\Delta\theta^*) - y_1' * \sin(\Delta\theta^*)\right)\\ \Delta y_1 &= y_1 - r^* \left(x_1' * \sin(\Delta\theta^*) + y_1' * \cos(\Delta\theta^*)\right).\end{aligned} \quad (5)$$

Then, most of the outliers are eliminated according to the following logical filter [11]:

$$|\Delta x_1 - \Delta x^*| \geq \Delta x_{\mathrm{th}},\ |\Delta y_1 - \Delta y^*| \geq \Delta y_{\mathrm{th}} \quad (6)$$

where Δx_{th} and Δy_{th} denote, respectively, the thresholds of horizontal and vertical differences. The thresholds are set to the bin widths of corresponding histograms [11]. Finally, we get a keypoint pair set PP_2 from PP_1, and the FSC algorithm [15] is used to find correct correspondences from keypoint pair set PP_2.

Note that although we need to compute the Euclidean distance for every keypoint pair in the initial matching step, we save computational efforts in the rematching step. To display the distribution of histograms well, d_{ratio} is set to 0.9. To get as many candidate keypoint pairs as possible, d_r is set to 0.9 [4]. The FSC algorithm employed in the outlier removal step can get more correct matches than random sample consensus [16] in fewer iterations.

IV. Experiment and Result

A. Test Image Pairs

To evaluate the proposed method, three image pairs are tested. These image pairs are shown in Fig. 1. The first pair P-A is multispectral images from the U.S. Geological Survey project [17], Lat/Long: 69.6/−92.7, 240-m resolution. A segment with a size of 614 × 611 from band 5 (Sensor: Landsat-7 ETM+, Date: 2000/7/24) was selected as the reference image. To increase the difficulty of the test data set, a segment with a size of 614 × 611 from band 3 (Sensor: Landsat 4-5 TM, Date: 1999/6/28) after a simulated rotation of 90° was selected as the sensed image. The second pair P-B is two 412 × 300 multisensor images with the reference image obtained from band 5 of a scene taken by the sensor Landsat-TM in September 1995 (with a spatial resolution of 30 m), and the sensed image is the optical image obtained from Google earth (with a spatial resolution of 5 m). The third pair P-C is two 800 × 800 multisensor images with the reference image obtained from the HH mode (L-band) of a scene taken by the sensor ALOS-PALSAR on June 5, 2010, in the region of Campbell River in British Columbia (with an initial spatial resolution of 15 m resampled to 30 m), and the sensed image is from band 5 (1.55–1.75 μm) of a scene taken by the sensor Landsat-ETM+ on June 26, 1999, in the same region (with a spatial resolution of 30 m).

B. Evaluation Criterion

1) Matching Accuracy: The accuracy is evaluated by the root-mean-square error (rmse) criterion [2], [11]. A total of N corresponding point pairs $\{(x_i, y_i), (x_i', y_i')\}$ are manually selected from the reference and sensed images. The point pairs are carefully chosen and are refined to reduce the residual as low as possible [2]. Hence, those point pairs are used as the reference to test the precision of model parameters. The rmse is computed according to

$$\mathrm{RMSE} = \sqrt{\frac{1}{N}\sum_{i=1}^{N}\left(x_i - x_i''\right)^2 + \left(y_i - y_i''\right)^2} \quad (7)$$

where (x_i'', y_i'') denotes the transformed coordinates of (x_i', y_i'). For each test image pair, the algorithm is executed ten times, and the average of the ten results is computed as the final result.

2) Keypoint Number: The number of correct correspondences is used as the criterion to evaluate the robustness of the proposed method [18]. The thresholds for keypoint detection are adjusted, so the comparison method and the proposed method have roughly the same number of detected points.

C. Experimental Results

We compare the proposed PSO-SIFT algorithm with the SIFT-based FSC algorithm, SURF, SAR-SIFT [14], and the MS-SIFT algorithm. Although the SAR-SIFT algorithm is specifically designed for SAR images, it shows a good performance for other types of remote sensing images. In addition to SURF, other methods are implemented under MATLAB R2012a with an Intel Core 2.53-GHz processor and 6 GB of physical memory. The source code is available at https://github.com/ZeLianWen/Image-Registration.

The results of matching accuracy, correctly matched keypoint number, and the average running time for three test pairs are shown in Table I. Note that the algorithm is executed ten times and the average of the ten running time as the final running time. The test pair P-A is acquired in two different bands and different sensor devices. Due to the different spectral bands, there are some irregular relations of the intensity mapping between the remote image pair. Considering the results in Table I, SIFT, SAR-SIFT, and SURF fail to register the test pair P-A. However, after we modified the gradient calculation method, 121 correctly matched keypoints are filtered, and the subpixel matching results are achieved, which indicate the robustness of the new gradient definition. Although the MS-SIFT can accurately match the test pair P-A, it is difficult to tune its parameters to obtain satisfactory results. The test pairs P-B and P-C are acquired with different sensor devices, and there are monotonic relations of the image intensity between the remote image pairs. SIFT, SURF, SAR-SIFT, and MS-SIFT can accurately match this image pair, indicating that those methods are invariant to monotonic intensity transform. The proposed gradient calculation method also achieves subpixel accuracy. To verify the robustness of the enhanced feature matching method, we compare two algorithms that are named as Proposed gradient + FSC and Proposed gradient + Enhanced matching. It can be clearly seen that the enhanced matching method effectively increases the number of correctly matched keypoints. For test image pair P-A, though the RMSE of enhanced matching is a

This article has been accepted for inclusion in a future issue of this journal. Content is final as presented, with the exception of pagination.

TABLE I
COMPARISON OF RMSE, CORRECTLY MATCHED NUMBER, AND AVERAGE RUN TIME FOR TEST IMAGES

Method	P-A (size: 614×611)			P-B (size: 412×300)			P-C (size: 800×800)		
	RMSE	N	Times(s)	RMSE	N	Times(s)	RMSE	N	Times(s)
SIFT+FSC($d_{ratio} = 0.9$)	*	*	36.14	0.7041	33	19.96	0.5884	59	48.09
SURF($d_{ratio} = 0.8$)	*	*	1.11	1.6324	10	0.53	0.9553	51	1.35
SAR-SIFT($d_{ratio} = 0.9$)	*	*	60.99	1.5042	11	16.39	0.6146	117	105.79
MS-SIFT($d_{ratio} = 1$)	0.5952	104	39.26	0.7018	55	12.79	0.6483	58	46.31
Proposed gradient+FSC($d_{ratio} = 0.9$)	0.5508	121	44.09	0.6910	27	20.16	0.5662	54	54.55
Proposed gradient+Enhanced matching ($d_{ratio} = 0.9, d_r = 0.9$)(**proposed**)	**0.5732**	**177**	**52.03**	**0.6718**	**75**	**23.02**	**0.5403**	**85**	**62.6**

*: Fails to register the image pair(RMSE>4)

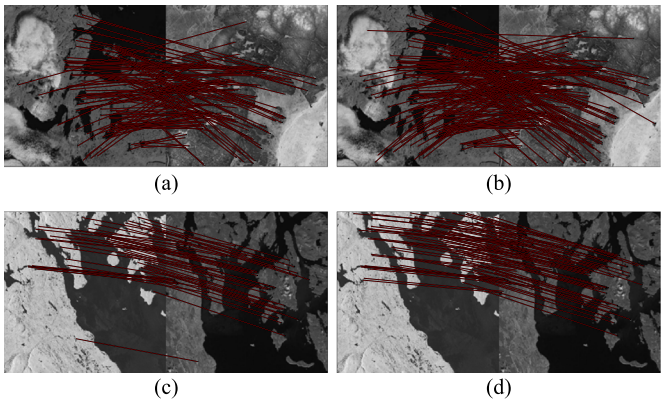

Fig. 5. Matching results of Fig. 1. (a) and (c) Proposed gradient + FSC. (b) and (d) Proposed gradient + Enhanced matching.

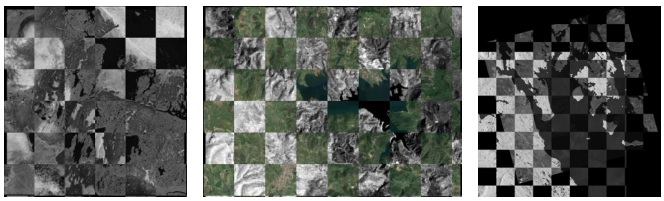

Fig. 6. Checkerboard mosaiced images of the proposed method. (a) Result for the image pair P-A. (b) Result for the image pair P-B. (c) Result for the image pair P-C.

little higher than FSC, it also achieves sub-pixel accuracy. The robustness of the FSC algorithm is also proved. Because of the realization of SURF based on C++, the efficiency is very high. The matching results of two image pairs are shown in Fig. 5. Compared with FSC, the enhanced matching method greatly increases the correct matches. The checkerboard mosaiced images are shown in Fig. 6. It can be seen that the edge and region of two images are precisely overlapped, which demonstrates the accuracy of our proposed method.

V. CONCLUSION

In this letter, we have proposed a new gradient computation method that is more robust to complex nonlinear intensity transform of remote sensing images. In addition, a robust point matching algorithm that combines the position, scale, and orientation of each keypoint to increase the number of correct correspondences has been proposed. Experimental results on multispectral and multisensor remote sensing images show that our method reveals better performance than the state-of-the-art methods in terms of aligning accuracy and correctly matched number of keypoints in some cases.

REFERENCES

[1] A. Wong and D. A. Clausi, "ARRSI: Automatic registration of remote sensing images," *IEEE Trans. Geosci. Remote Sens.*, vol. 45, no. 5, pp. 1483–1493, May 2007.
[2] M. Gong, S. Zhao, L. Jiao, D. Tian, and S. Wang, "A novel coarse-to-fine scheme for automatic image registration based on sift and mutual information," *IEEE Trans. Geosci. Remote Sens.*, vol. 52, no. 7, pp. 4328–4338, Jul. 2014.
[3] A. Sedaghat, M. Mokhtarzade, and H. Ebadi, "Uniform robust scale invariant feature matching for optical remote sensing images," *IEEE Trans. Geosci. Remote Sens.*, vol. 49, no. 11, pp. 4516–4527, Nov. 2011.
[4] Q. Li, G. Wang, J. Liu, and S. Chen, "Robust scale-invariant feature matching for remote sensing image registration," *IEEE Geosci. Remote Sens. Lett.*, vol. 6, no. 2, pp. 287–291, Apr. 2009.
[5] J. Senthilnath, S. N. Omkar, V. Mani, and T. Karthikeyan, "Multiobjective discrete particle swam optimization for multisensor image alignment," *IEEE Geosci. Remote Sens. Lett.*, vol. 10, no. 5, pp. 1095–1099, Sep. 2013.
[6] J. Senthilnath, N. P. Kalro, and J. A. Benediktsson, "Accurate point matching based on multi-objective genetic algorithm for multi-sensor satellite imagery," *Appl. Math. Comput.*, vol. 236, pp. 546–564, 2014.
[7] D. G. Lowe, "Distinctive image features from scale-invariant keypoints," *Int. J. Comput. Vis.*, vol. 60, no. 2, pp. 91–110, Nov. 2004.
[8] H. Bay, A. Ess, and T. Tuytelaars, "SURF: Speeded-up robust features," *Comput. Vis. Image Understand.*, vol. 110, no. 3, pp. 346–359, Jun. 2008.
[9] K. Mikolajczyk and C. Schmid, "A performance evaluation of local descriptors," *IEEE Trans. Pattern Anal. Mach. Intell.*, vol. 27, no. 10, pp. 1615–1630, Oct. 2005.
[10] S. Leutenegger, M. Chli, and R. Siegwart, "BRISK: Binary robust invariant scalable keypoints," in *Proc. IEEE Int. Conf. Comput. Vis.*, 2011, pp. 2548–2555.
[11] B. Kufer, N. S. Netanyahu, and I. Shimshoni, "An efficient SIFT-based mode-seeking algorithm for sub-pixel registration of remotely sensed images," *IEEE Geosci. Remote Sens. Lett.*, vol. 12, no. 2, pp. 379–383, Feb. 2015.
[12] Q. Yang and X. Xiao, "A new registration method base on improved Sobel and SIFT algorithms," in *Proc. 3rd Int. Conf. Comput. Elect. Eng.*, 2010, p. 528.
[13] Y. Li, L. Liu, L. Wang, D. Li, and M. Zhang, "Fast SIFT algorithm based on Sobel edge detector," in *Proc. 2nd Int. Conf. Consum. Electron, Commun. Netw.*, Apr. 2012, pp. 1820–1823.
[14] F. Dellinger, J. Delon, Y. Gousseau, J. Michel, and F. Tupin, "SAR-SIFT: A SIFT-like algorithm for SAR images," *IEEE Trans. Geosci. Remote Sens.*, vol. 53, no. 1, pp. 453–466, Jan. 2015.
[15] Y. Wu, W. Ma, M. Gong, L. Su, and L. Jiao, "A novel point-matching algorithm based on fast sample consensus for image registration," *IEEE Geosci. Remote Sens. Lett.*, vol. 12, no. 1, pp. 43–47, Jan. 2015.
[16] M. A. Fischler and R. C. Bolles, "Random sample consensus: A paradigm for model fitting with applications to image analysis and automated cartography," *Commun. ACM*, vol. 24, no. 6, pp. 381–395, Jun. 1981.
[17] [Online]. Available: http://glovis.usgs.gov/
[18] Q. Li, S. Qi, Y. Shen, D. Li, H. Zhang, and T. Wang, "Multispectral image alignment with nonlinear scale-invariant keypoint and enhanced local feature matrix," *IEEE Geosci. Remote Sens. Lett.*, vol. 12, no. 7, pp. 1551–1556, Jul. 2015.